Cell Reports

Article

Nutrient-Dependent Trade-Offs between Ribosomes and Division Protein Synthesis Control Bacterial Cell Size and Growth

Graphical Abstract

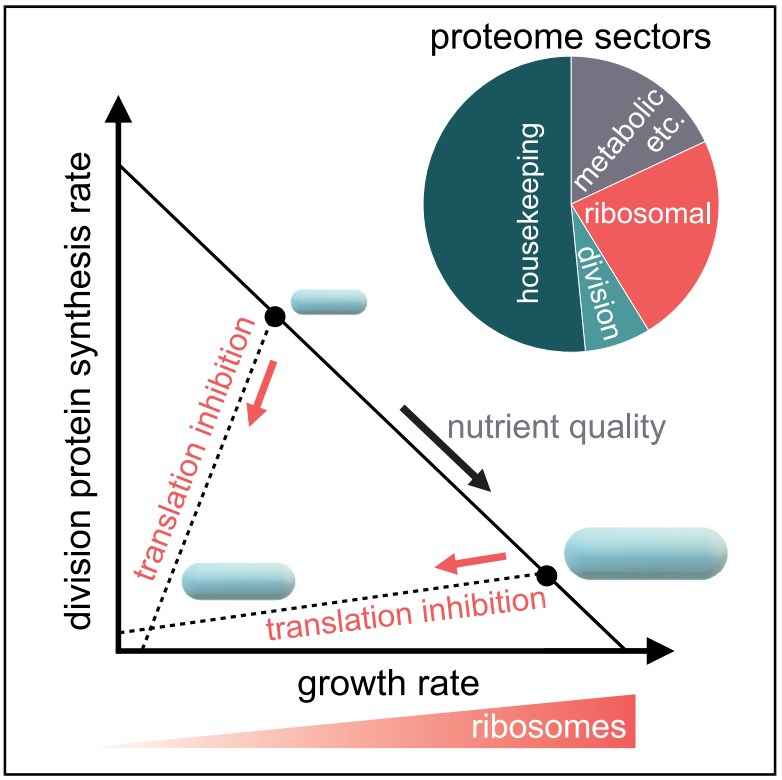

Authors

Diana Serbanescu, Nikola Ojkic, Shiladitya Banerjee

Correspondence

shiladtb@andrew.cmu.edu

In Brief

How protein synthesis regulates cell size remains poorly understood. Serbanescu et al. show that cell size is controlled by a trade-off between the allocation of cellular resources toward ribosomal and division protein synthesis. This principle quantitatively determines bacterial cell morphology and growth rates under nutrient shifts or translational perturbations.

Highlights

- A trade-off between ribosomal and division protein synthesis sets bacterial size
- In nutrient-poor media, cells grow larger under translation inhibition
- Fast-growing cells spend more resources on division under translation inhibition
- Bacteria actively regulate cell size and shape to promote fitness under stress

Serbanescu et al., 2020, Cell Reports *32*, 108183
September 22, 2020
https://doi.org/10.1016/j.celrep.2020.108183

CellPress

Cell Reports

CellPress
OPEN ACCESS

Article

Nutrient-Dependent Trade-Offs between Ribosomes and Division Protein Synthesis Control Bacterial Cell Size and Growth

Diana Serbanescu,[1,2] Nikola Ojkic,[1,2] and Shiladitya Banerjee[3,4,*]
[1]Department of Physics and Astronomy, University College London, London WC1E 6BT, UK
[2]Institute for the Physics of Living Systems, University College London, London WC1E 6BT, UK
[3]Department of Physics, Carnegie Mellon University, Pittsburgh, PA 15213, USA
[4]Lead Contact
*Correspondence: shiladtb@andrew.cmu.edu
https://doi.org/10.1016/j.celrep.2020.108183

SUMMARY

Cell size control emerges from a regulated balance between the rates of cell growth and division. In bacteria, simple quantitative laws connect cellular growth rate to ribosome abundance. However, it remains poorly understood how translation regulates bacterial cell size and shape under growth perturbations. Here, we develop a whole-cell model for growth dynamics of rod-shaped bacteria that links ribosomal abundance with cell geometry, division control, and the extracellular environment. Our study reveals that cell size maintenance under nutrient perturbations requires a balanced trade-off between ribosomes and division protein synthesis. Deviations from this trade-off relationship are predicted under translation inhibition, leading to distinct modes of cell morphological changes, in agreement with single-cell experimental data on *Escherichia coli*. Furthermore, by calibrating our model with experimental data, we predict how combinations of nutrient-, translational-, and shape perturbations can be chosen to optimize bacterial growth fitness and antibiotic resistance.

INTRODUCTION

Cell size maintenance is essential for regulating cell physiology, function, and fitness (Young, 2006). Maintaining a characteristic cell size necessitates an intricate balance between cell growth and division rates. How this balance is achieved in different growth conditions remains an outstanding question. It has been known for over six decades that bacteria modulate their size in response to changes in nutrient conditions. Quantifying the cell size and growth rates of *Salmonella enterica* grown in different nutrient media, Schaechter et al. (1958) discovered the *nutrient growth law*—bacterial cell size increases exponentially with the population growth rate. High-throughput single-cell studies in recent years have confirmed this result for evolutionary divergent *Escherichia coli* and *Bacillus subtilis* (Sauls et al., 2019; Si et al., 2017; Taheri-Araghi et al., 2015; Vadia and Levin, 2015), suggesting common strategies for bacterial cell size control. However, single-cell data show deviations from the nutrient growth law in experiments altering cellular proteomics (Basan et al., 2015b; Si et al., 2017), leaving open the connection between cell size, growth rate, and protein synthesis.

At the single-cell level, cell size homeostasis is achieved via the *adder* mechanism, whereby cells add a constant volume between consecutive division events, irrespective of the cell size at birth (Amir, 2014; Banerjee et al., 2017; Taheri-Araghi et al., 2015; Wallden et al., 2016). As a result of this strategy, cells deviating from the average homeostatic size quickly converge to the average size within a few generations (Campos et al., 2014; Deforet et al., 2015; Jun and Taheri-Araghi, 2015; Sauls et al., 2016; Taheri-Araghi et al., 2015). This strategy for cell size homeostasis is followed by a wide range of bacterial species including *E. coli*, *B. subtilis*, *C. crescentus*, and *Pseudomonas aeruginosa* (Campos et al., 2014; Deforet et al., 2015; Jun and Taheri-Araghi, 2015; Osella et al., 2014; Taheri-Araghi et al., 2015), but it does not reveal a molecular-level understanding of the mechanism for cell size control (Jun et al., 2018).

Two distinct types of regulatory models have been proposed in recent years for the control of bacterial cell size. The first is the replication-initiation-centric model: cell size control is set by the time period of chromosome replication and the subsequent cell division ($C+D$ period; Donachie, 1968; Ho and Amir, 2015; Wallden et al., 2016). The second is the division-centric model: cell size is regulated by the accumulation of a threshold amount of cell envelope precursors (Harris and Theriot, 2016) or division proteins (e.g., FtsZ; Ojkic et al., 2019; Si et al., 2019). In replication-initiation-centric models, cell size at division is determined by the $C+D$ period, but it remains poorly understood how $C+D$ periods are modulated by growth rate perturbations targeting nutrient quality, translation or protein expression. Recent studies have challenged the replication-initiation-centric models for cell size control (Micali et al., 2018a, 2018b; Grilli et al., 2018; Si et al., 2019), suggesting concurrence of

replication initiation and division processes (Micali et al., 2018a). In particular, experiments have demonstrated that replication initiation and cell division are independently controlled in *E. coli* and *B. subtilis* (Si et al., 2019), and data support a model in which cell division is triggered by the accumulation of a threshold amount of division proteins (Deforet et al., 2015; Ghusinga et al., 2016). However, it remains unknown how the synthesis of division proteins is altered by nutrients or translational perturbations to regulate cell size.

A key component in understanding cell size regulation is the interdependence between growth rate and the macromolecular composition of the cell. The nutritional content of the growth medium sets the specific growth rate (Schaechter et al., 1958; Scott et al., 2014), which in turn regulates the macromolecular composition of cells (Kaczanowska and Rydén-Aulin, 2007; Klumpp et al., 2013). For exponentially growing *E. coli* cells, RNA and ribosome abundance increase linearly with the growth rate (Maaløe, 1979; Yin, 2004; Ecker and Schaechter, 1963; Zaslaver et al., 2009; Basan et al., 2015b; Harvey, 1973). This implies an upregulation in translation leading to increased protein production for growth (Basan et al., 2015b; Kjeldgaard et al., 1958; Schaechter, 2006) and cell size inflation. While this model is in agreement with experimental observations for cell size increasing with increasing nutrient concentrations, it fails to explain cell size changes under translation inhibition (Basan et al., 2015b; Si et al., 2017). In particular, it remains unclear whether translation inhibition would lead to an increase in cell size such that there is a positive correlation between cell size and ribosome abundance, or a decrease in cell size with growth-rate reduction. Both these behaviors are observed in experiments (Si et al., 2017). To explain how translation and nutrient quality regulate cell morphologies, we develop a whole-cell, coarse-grained theory that links ribosomes with cell geometry, division control, and the extracellular environment.

Our theoretical framework combines a mechanistic model of cell shape and division with an extended ribosomal-resource-allocation model, allowing us to quantitatively predict cell size changes under nutrient shifts and translational perturbations. We use ribosome abundance as the one of the key regulatory variables, as approximately 85% of cellular RNA encodes for rRNA that is folded in ribosomes (Bremer and Dennis, 1996; Scott et al., 2010). We also assume that all the nutrients transported from the extracellular medium into the cell are used in the production of ribosomes and other proteins. This is because over 80% of cell's energy budget for biomass is spent on rRNA and protein synthesis (Stouthamer and Bettenhaussen, 1973). Using this framework, we uncover a model for balanced allocation of ribosomal resources toward cell growth and division. We find that a balanced trade-off between the rates of cell growth and division proteins synthesis sets bacterial size under nutrient shifts. As a result, in rich media, cells produce division proteins more slowly than they elongate cells, leading to larger cell sizes.

We then extend our framework to predict cell morphologies under translation inhibition across different nutrient media. Our model predicts three different types of cell morphological response unifying past experimental observations (Basan et al., 2015b; Scott et al., 2010; Si et al., 2017). First, cells deprived of nutrients allocate more ribosomes toward growth, which results in an increase in volume. Second, cells grown in nutrient-rich media favor resource allocation toward division, and thus a decrease in volume is observed under translation inhibition. Under optimal growth conditions, cells preserve the balance between growth and division protein synthesis, such that cell size is invariant under translational perturbations. We show that cell size changes are intimately coupled to the regulation of cell surface-to-volume ratio that controls nutrient and antibiotic influx rates. We therefore investigate the relationship among cell shape, nutrient quality, and bacterial growth rate under translational perturbations. We predict that round cells are most resistant to translation-inhibitory antibiotics, and that drug resistance increases with increasing nutrient quality. Thus, induced filamentation could have a negative impact on bacterial growth fitness (Miller et al., 2004), whereas cell rounding could promote bacterial resistance to ribosome-targeting antibiotics.

RESULTS

Cell Size Control Emerges from Nutrient-Dependent Trade-Off between Rates of Cellular Growth and Division Protein Synthesis

To understand how bacterial cell size changes with the nutrient-specific growth rate, we develop a model for the allocation of ribosomal resources toward cell growth and division protein synthesis. During each cell cycle, cells elongate exponentially in volume (V) at a rate κ. At steady state, κ depends linearly on the ribosomal mass fraction r ($\approx$RNA/protein ratio), such that

$$\frac{dV}{dt} = \kappa(r)V(t)\,, \tag{1}$$

where $\kappa(r) = \kappa_t(r - r_{\min})$ (Scott et al., 2010). Here, κ_t can be interpreted as the translational capacity of the cell, which correlates with the speed of translational elongation (Ruusala et al., 1984), and $r_{\min}$ is the minimum RNA/protein ratio needed for growth (Figure 1C, inset). The value for $r_{\min}$ is obtained from the intercept of κ as a function of r from experimental data (Scott et al., 2010; Si et al., 2017).

We combine this model for growth with a model for the control of cell division (Figure 1A). The division proteins, X, are synthesized at a rate proportional to the cell volume and degraded at a rate μ:

$$\frac{dX}{dt} = k_p(r)V(t) - \mu X(t)\,, \tag{2}$$

where $k_p(r)$ is the rate of synthesis of division proteins that is assumed to be a function of the ribosome mass fraction r. Cell division is triggered when a threshold copy number of division proteins, X_0, is accumulated at the mid-plane of the cell (Figure 1B). While various proteins could be potential candidates for division initiation (Adams and Errington, 2009; Bi and Lutkenhaus, 1991; Flåtten et al., 2015; Robert, 2015), a recent study identifies FtsZ as the key initiator protein that assembles a ring-like structure in the mid-cell region to trigger septation (Si et al., 2019). We therefore suggest that X represents FtsZ copy

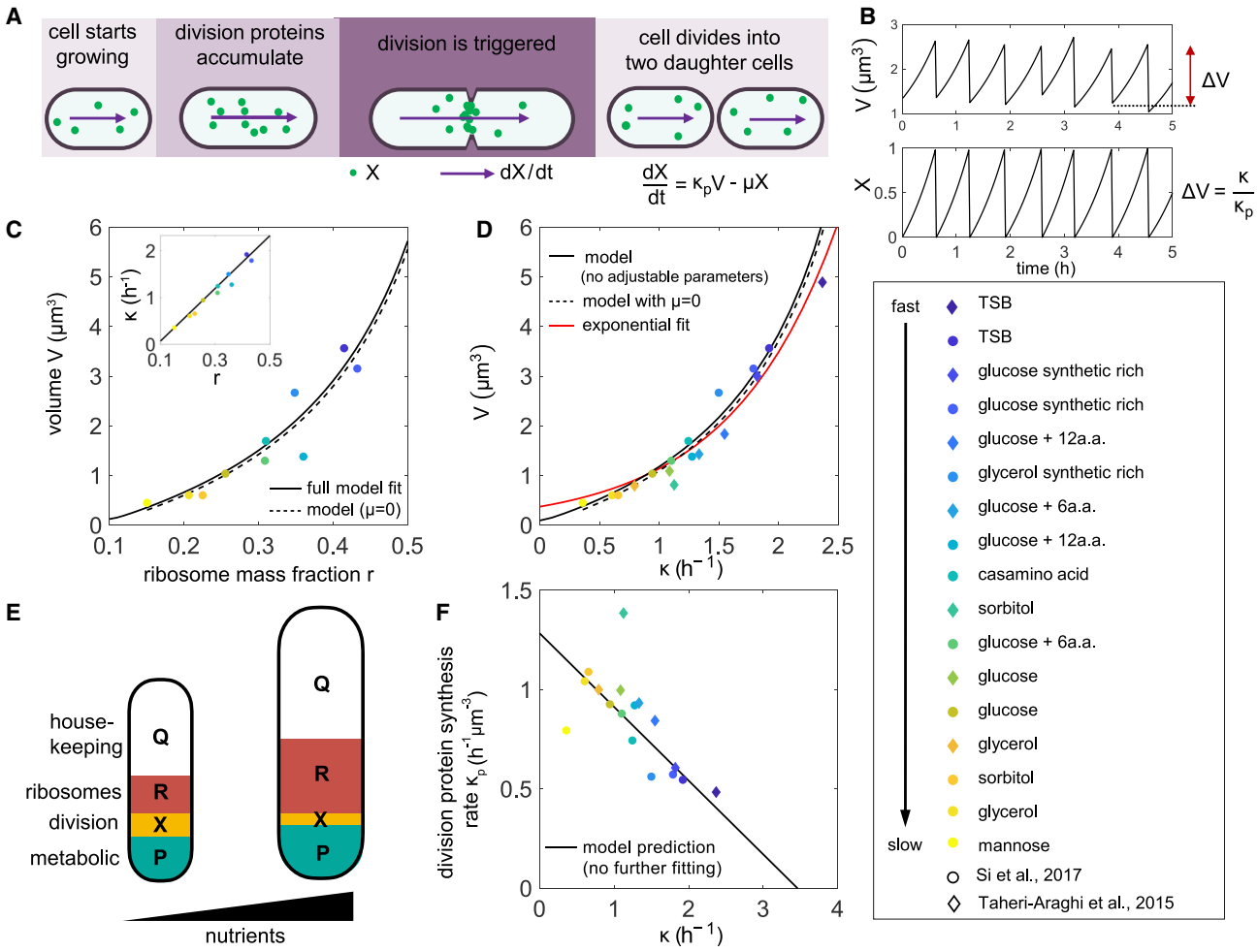

Figure 1. Cell Size Control under Nutrient Perturbations

(A) Schematic of the threshold initiation model. Once a threshold amount of division proteins, X, is accumulated, cell division is triggered. Division proteins are synthesized at a rate κ_p per unit volume.

(B) Dynamics of cell volume and normalized fraction of division proteins show that the average added volume between consecutive division events is constant, consistent with the phenomenological adder model.

(C) Fitted model for average cell volume as a function of ribosome mass fraction. Solid line: full model fit with X protein degradation; dashed line: approximate model with no X degradation ($\mu = 0$). Inset: fitted linear relationship $\kappa = \kappa_t(r - r_{min})$ (Scott et al., 2010).

(D) Model prediction for the relationship between the average cell volume and growth rate compared against an exponential fit as predicted by the nutrient growth law (Schaechter et al., 1958).

(E) Schematic representation of the proteome allocation model, showing ribosomal trade-off between cell growth and division protein synthesis for cells growing in poor and rich nutrient media.

(F) Negative correlation between the rate of division protein synthesis and growth rate, as predicted by the model. Experimental data are obtained from Si et al. (2017) and Taheri-Araghi et al. (2015). In the experimental data, κ_p is estimated from the ratio $\kappa/\langle V\rangle$. See Table 1 for a complete list of parameter values. See also Figures S1 and S2.

number and assume that its turnover rate in the ring-bound state is much faster than its rate of synthesis (Söderström et al., 2018). As a result, all the newly synthesized FtsZs in the cytoplasm are assumed to be recruited in the ring. We note that the degradation of X is consistent with reports of active degradation of FtsZ by ClpXP (Männik et al., 2018; Sekar et al., 2018; Si et al., 2019).

Solving Equations 1 and 2, we obtain: $X_0 = (V_d - V_b 2^{-\mu/\kappa})k_p/(\kappa + \mu)$, where V_b and V_d are the cell volumes at birth and division, respectively. In the limit $k \gg \mu$, we get $X_0 = \Delta V k_p/\kappa$, where $\Delta V = V_d - V_b$ is the added volume per generation. As X_0, k_p and κ are constant for a given growth medium, and cells add a constant volume ΔV in each growth generation, consistent with the phenomenological adder model. Conversely, in the limit $k \ll \mu$, $V_d \approx X_0\mu/k_p$ is consistent with data that *E. coli* deviates from an adder in slow-growing media (Wallden et al., 2016; Si et al., 2019). Furthermore, for symmetrically dividing bacterium, the average newborn cell volume, $\langle V_b\rangle$, asymptotes to ΔV . Therefore, average cell volume $\langle V\rangle$ in a given growth medium is given by

$$\langle V\rangle = \frac{\kappa+\mu}{\kappa_p(2-2^{-\mu/\kappa})}\ , \tag{3}$$

where $\kappa_p = k_p/(2X_0\ln 2)$ is the normalized rate of division protein synthesis. Thus, cell volume can be modulated by perturbations in translation, as both κ and κ_p are functions of the ribosomal mass fraction. A key proposition of our model is that there is a trade-off between ribosomes allocated for synthesizing growth and division proteins such that

$$\kappa_p = \kappa_p^0\left(r^*_{\max} - r\right)\ , \tag{4}$$

where we interpret κ_p^0 as the rate of production of FtsZ per ribosomes, and $r^*_{\max}$ is the ribosome mass fraction when growth rate is maximum. We note that the parameter κ_p^0 can be perturbed by translation, whereas $r^*_{\max}$ is regulated by both translational and nutrient capacities of the cell, as derived in the following section (see STAR Methods for further details). By combining the expressions for growth rate and division protein synthesis rate, we find

$$\langle V\rangle = \frac{\kappa_t(r-r_{\min})+\mu}{\kappa_p^0\left(r^*_{\max}-r\right)\left(2-2^{-\mu/\kappa(r)}\right)}\ , \tag{5}$$

such that average cell size increases with increasing ribosome abundance. We fit the expression in Equation 5 to experimental data (Si et al., 2017) to determine the parameters κ_p^0, μ, and $r^*_{\max}$ (Figure 1C, solid line). Importantly, we find that $\mu = 0.24\ \mathrm{h}^{-1}$, allowing us to approximate the average volume as the ratio of growth rate to the rate of division protein synthesis: $\langle V\rangle \approx \kappa/\kappa_p = (\kappa_t(r-r_{\min})/\kappa_p^0(r^*_{\max}-r))$ (Figure 1C, dashed line). Thus κ_p can be indirectly measured from $\kappa/\langle V\rangle$ data across different growth conditions. Direct measurement of κ_p would necessitate measuring the rate of change in FtsZ fluorescence intensity per unit cell volume during cell division cycles.

We can then express the average cell volume as a function of nutrient-specific growth rate, recapitulating the *nutrient growth law* of Schaechter et al. (1958) that cell size increases monotonically with increasing growth rate:

$$\langle V\rangle = \frac{\kappa}{\kappa_p^0\left(r^*_{\max}-r_{\min}\right)-\frac{\kappa_p^0}{\kappa_t}\kappa}\ . \tag{6}$$

With no further fitting, we directly compare the prediction in Equation 6 with experimental data for *E. coli* cell volume under nutrient perturbations (Figure 1D). The result in Equation 6 deviates from the phenomenological model of exponential dependence between cell size and growth rate, and predicts a maximum growth rate, $\kappa_{\max} = \kappa_t(r^*_{\max}-r_{\min}) \approx 3.1\ \mathrm{h}^{-1}$, when all ribosomal resources are allocated toward growth. Our model captures the departure from an exponential relationship between cell size and growth rate for $\kappa < 0.7\ \mathrm{h}^{-1}$, as recently reported by Zheng et al., 2020 (Figure S1A). We find that a linear relationship between cell size and growth rate does not accurately capture the cell size data for the range of growth rates studied in this work.

Mechanistic Origin of Ribosomal Trade-Off between Growth and Division

To understand the mechanistic origin of the ribosomal trade-off between growth and division protein synthesis (Equation 4), we develop a model for allocation of ribosomal resources, extending the framework of Scott et al. (2010). The total protein content of the cell can be decomposed into four classes (Figure 1E): ribosome-affiliated proteins (R, mass fraction ϕ_R); housekeeping proteins not affected by translation (Q, mass fraction ϕ_Q); division proteins (X, mass fraction ϕ_X); and the rest are non-ribosomal proteins that constitute the P-sector (P, mass fraction ϕ_P). The mass fractions are constrained by the equation $\phi_R + \phi_X + \phi_P = 1 - \phi_Q = \phi_R^{\max} = \text{constant}$. For different combinations of the nutritional and translation capacities of the cell, efficient resource allocation requires that the abundance of P- and R-class proteins be adjusted so that the rate of nutrient influx by P matches the rate of protein synthesis achievable by R: $\kappa_n\phi_P = \kappa_t(\phi_R - \phi_R^{\min})$, where κ_n is the nutritional capacity of the cell. This results in the following relation between the mass fractions of ribosomes and division proteins:

$$\frac{\phi_R-\phi_R^{\min}}{\phi_R^{\max}-\phi_R-\phi_X} = \frac{\kappa_n}{\kappa_t}\ , \tag{7}$$

predicting a negative correlation between ϕ_X and ϕ_R under nutrient or translational perturbations (Figure S1C). Using a dynamic proteome sector model (STAR Methods), we can derive that the rate of production of division proteins, κ_p, is proportional to ϕ_X during steady-state growth. Using $r = \phi_R/\rho$, where ρ is a constant conversion factor, we derive the negative correlation between κ_p and r, as assumed in Equation 4,

$$\kappa_p \propto \kappa_t\left(\phi_R^{\max}-\phi_R^{\min}\right)\left(\frac{\kappa_n\phi_R^{\max}+\kappa_t\phi_R^{\min}}{\rho(\kappa_n+\kappa_t)}-r\right)\ , \tag{8}$$

where we identify $\kappa_p^0 \propto \kappa_t(\phi_R^{\max}-\phi_R^{\min})$ and $r^*_{\max} = (\kappa_n\phi_R^{\max}+\kappa_t\phi_R^{\min})/\rho(\kappa_n+\kappa_t)$ (see details in STAR Methods). Thus the trade-off between ribosomes and division protein synthesis naturally emerges in the extended proteome allocation model. Growth rate κ decreases with increased allocation of resources toward division proteins ϕ_X (Figures 1E, 1F, and S1D):

$$\kappa = \frac{\kappa_n\kappa_t}{\kappa_n+\kappa_t}\left(\phi_R^{\max}-\phi_R^{\min}-\phi_X\right)/\rho\ . \tag{9}$$

With all the model parameters inferred from experimental data (STAR Methods; Table 1), we can plot the dependency of κ_p on κ (Figure 1F), showing the negative correlation between the rate of division protein synthesis and the rate of volumetric growth, and directly predict the dependency of cell volume on growth rate (Figure S1B). Cells growing in nutrient-poor medium allocate a smaller fraction of ribosomes toward growth, resulting in smaller size on average. However, cells growing in nutrient-rich medium inflate their size by allocating a larger fraction of ribosomes toward growth (Figure 1E).

Table 1. List of Parameters Used in Models of Growth Perturbations

Parameter	Value	Growth Medium	Expression/ Method Used	Figure Number
r_{min}	0.1	all	$\kappa = \kappa_t(r - r_{min})$	Figures 1, 2, 3, and 4
$\kappa_t(h^{-1})$	5.6	all	Equation 5	Figures 1, 2, 3, and 4
$\kappa_p^0(h^{-1}\ \mu m^{-3})$	2.1	all		
r^*_{max}	0.7	all		
$\mu(h^{-1})$	0.24	all		Figure 1
$r_{max} - r_X$	0.76	Tryptic Soy Broth (TSB)	$\kappa = \kappa_n(r_{max} - r_X - r)$	Figures 2, 3, and 4
	0.92	synthetic rich		
	0.76	glucose + 12 amino acid (aa)		
	0.54	casamino acid		
	0.58	glucose + 6 aa		
	0.74	glucose		
	0.64	glycerol		
	0.29	sorbitol		
	0.23	mannose		
$\kappa_n(h^{-1})$	9.1	TSB	$\kappa_p = \frac{\kappa_p^0}{\kappa_n}\kappa + \kappa_p^0\delta r$	Figures 2, 3, and 4
	8.9	synthetic rich		
	3.4	glucose + 12 aa		
	3.5	casamino acid		
	3.4	glucose + 6 aa		
	2.2	glucose		
	1.1	glycerol		
	1.6	sorbitol		
	1.4	mannose		
δr	0.37	TSB	$\kappa_p = \kappa_p^0(r_{max} - r_X + \delta r - r)$	Figures 2, 3, and 4
	0.13	synthetic rich		
	−0.18	glucose + 12 aa		
	0.08	casamino acid		
	−0.04	glucose + 6 aa		
	0.07	glucose		
	−0.1	glycerol		
	−0.4	sorbitol		
	−0.43	mannose		
$\kappa_m(h^{-1})$	2.6	all	$\kappa_n = \kappa_t\frac{\kappa}{\kappa_m - \kappa}$	Figure 2
$\kappa_r(h^{-1})$	0.6	all	calibrated	Figures 3 and 4
$\kappa_0(h^{-1})$	3	all	calibrated	Figures 3 and 4

Translation Inhibition Breaks Balanced Allocation of Ribosomal Resources

In a given nutrient medium, κ/κ_p is maintained at a constant value, indicating a balance between growth and division protein synthesis. If κ/κ_p remains invariant under translation inhibition, we expect cell size to remain unchanged, as previously suggested by Basan et al. (2015b). However, experimental data (Si et al., 2017) show that cell size could either increase, decrease, or remain unchanged when *E. coli* cells are subjected to varying concentrations of chloramphenicol—a ribosome-targeting antibiotic. We therefore hypothesize that translation inhibition breaks balanced allocation of ribosomal resources toward growth and division proteins, by differentially reducing the rates κ and κ_p.

Under translation inhibition, bacteria produce more ribosomes to compensate for the inactive ribosomes that are bound by antibiotics (Scott et al., 2010). By measuring bacterial growth rates (κ) and ribosome mass fractions (r) for increasing concentrations of chloramphenicol, Scott et al. (2010) found that κ linearly decreases with r. In the presence of a division protein sector, the relationship between κ and r is given by

$$\kappa = \kappa_n(r_{max} - r_X - r)\ , \qquad (10)$$

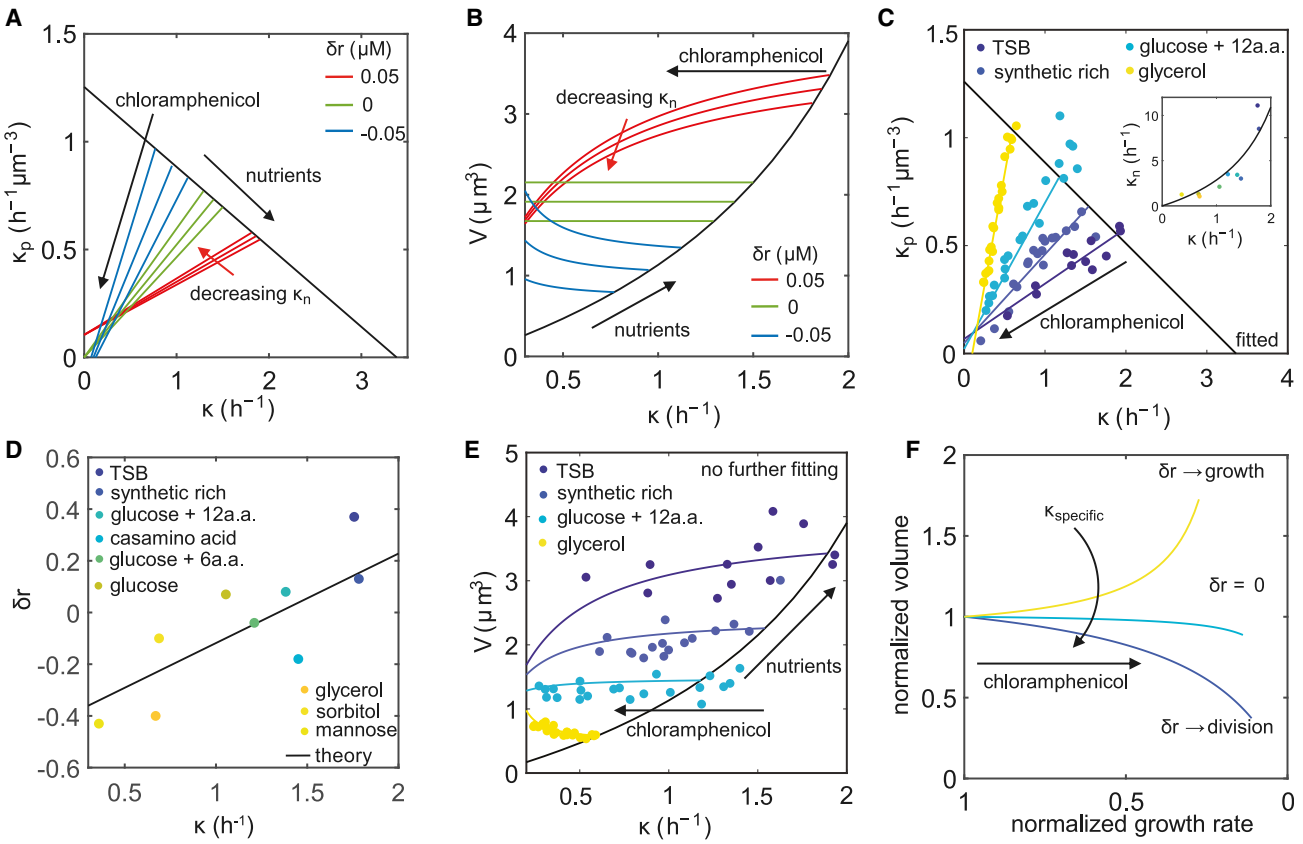

Figure 2. Cell Size Control under Translation Inhibition

(A) Model prediction for the dependence of division protein synthesis rate, κ_p, on growth rate, κ, under translation inhibition for three different values of δr. Decreasing κ_n corresponds to decreasing the nutrient quality of the growth medium.

(B) Model predictions for cell volume versus growth rate under translation inhibition, capturing three distinct trends in cell size changes depending on the value of δr.

(C) Model fit to experimental data for κ_p as a function of κ in three different nutrient conditions under translation inhibition. Inset: dependence of nutritional capacity κ_n on growth rate. Solid line is a fit of the form $\kappa_n = \kappa_t \kappa/(\kappa_m - \kappa)$, with the fitting parameter $\kappa_m = 2.6\ h^{-1}$.

(D) Dependence of δr on nutrient-specific growth rate. Solid line shows the theoretical prediction for the dependence of δr on nutrient-specific growth rate, $\delta r = -\frac{\kappa_m}{\kappa_t} + ((r_{max} - r_{min}/\kappa_m))\kappa$.

(E) Cell volume as a function of growth rate under translation inhibition.

(F) Three distinct morphological response to chloramphenicol, depending on the quality of nutrients. Volume and growth rates are normalized by their initial values before chloramphenicol is applied. In nutrient-rich media, cells allocate more ribosomes to division (dark blue line), thus increasing the surface-to-volume ratio to promote nutrient influx; whereas, in nutrient-poor media, they allocate more ribosomes toward growth, inflating the cell size (yellow line) and, in turn, decreasing the surface-to volume ratio to reduce the antibiotic influx. See Table 1 for a complete list of parameter values.

where κ_n is the nutritional capacity that depends on nutrient quality, $r_{max} = \phi_R^{max}/\rho$ is the maximum ribosome fraction that cells can produce under translation inhibition, and $r_X = \phi_X/\rho$ is the RNA/protein ratio devoted to synthesizing X proteins. By combining Equation 10 with Equation 4, we obtain

$$\kappa_p = \kappa_p^0(\kappa / \kappa_n + \delta r) \quad (11)$$

where $\delta r = r^*_{max} - r_{max} + r_X$ can be interpreted as the excess ribosomal mass fraction allocated to division protein synthesis under translation inhibition. By combining Equations 4, 7, and 10 we obtain a theoretical expression for the excess ribosomal mass fraction as a function of the growth rate: $\delta r = \kappa_n \Delta r/(\kappa_n + \kappa_t) - \kappa(\kappa_n + \kappa_t)/(\kappa_n \kappa_t)$, where $\Delta r = r_{max} - r_{min}$.

Since κ_n increases with κ (Figure 2C, inset), we predict that δr increases monotonically with nutrient-specific growth rate (Figure 2D, solid line).

Unlike nutrient perturbations, we find that κ_p and κ are positively correlated under translation inhibition (Figure 2A), such that they both decrease with increasing antibiotic concentration. Equation 11 can be combined with Equation 3 to determine how cell volume changes as a function of growth rate under translation inhibition:

$$\langle V \rangle = \frac{\kappa / \kappa_p^0}{\kappa/\kappa_n + \delta r}. \quad (12)$$

Interestingly, the above expression predicts three distinct behaviors (Figure 2B):

$$\begin{cases} \delta r > 0 \rightarrow r^*_{max} + r_X > r_{max}: & \text{excess ribosomes allocated to division, cell volume decreases;} \\ \delta r = 0 \rightarrow r^*_{max} + r_X = r_{max}: & \text{ribosomes equally shared between growth and division, cell volume is unchanged;} \\ \delta r < 0 \rightarrow r^*_{max} + r_X < r_{max}: & \text{more ribosomes allocated to growth, cell volume increases.} \end{cases}$$

We determine the parameters δr and κ_n for each growth medium, by fitting Equation 11 to the experimental data for κ_p versus cell growth rate κ under chloramphenicol perturbations (Si et al., 2017; Figure 2C). We find that $\delta r < 0$ in poor media and $\delta r > 0$ in rich growth media, whereas $\delta r \approx 0$ for cells growing with medium growth rates (Figure 2D). These data are consistent with our theoretical result that δr increases linearly with the nutrient-specific growth rate (Figure 2D, solid line). We interpret the above result as cells allocating excess ribosomes for growth in poor media, whereas, in rich media, cells tend to allocate more ribosomal resources for division protein synthesis. With no further adjustable parameters, our theory predicts the cell volume curves for each growth condition, which are in excellent quantitative agreement with the trend in the experimental data (Figure 2E).

Cells Actively Regulate Shapes to Adapt to Translational Perturbations

Under translation inhibition, decrease in cell volume in rich media is indicative of a higher surface-to-volume ratio that may increase the influx of nutrients and antibiotics. Conversely, in poor media, increase in cell volume may be indicative of a lower surface-to-volume ratio that in turn would reduce antibiotic and nutrient influx (Figure 2F). Therefore, surface-to-volume ratio of a cell may play a crucial role in controlling cellular adaptive response to growth perturbations, by modulating the relative rates of nutrient and antibiotic influx. To test the role of surface-to-volume ratio on bacterial growth, we construct a model coupling cell growth and geometry to nutrient and antibiotic transport.

Nutrient Dynamics

The dynamics of nutrient concentration inside the cell, $[n]$, is given by

$$\frac{d[n]}{dt} = J_n - \kappa[n] - \kappa_r r_a \tag{13}$$

where $J_n = [n_{ext}]P_{in}A/V$ is the nutrient influx, $[n_{ext}]$ is the nutrient concentration in the extracellular medium, P_{in} is the cell envelope permeability, and κ_r is the rate at which ribosomes are produced from the nutrients. The model for nutrient transport across the cell membrane is consistent with the one proposed in Pandey and Jain (2016) if we assume that the number of metabolic proteins (transporters) scales with the surface area of the cell. The interplay between nutrients and ribosome synthesis is schematically represented in Figure 3A. The intracellular concentration of nutrients determines the specific growth rate as: $\kappa_{specific} = \kappa_0[n]/([n] + n^*)$ (Monod, 1949), where κ_0 is the maximum growth rate characteristic of the medium, and n^* is the value of $[n]$ when $\kappa_{specific}/\kappa_0 = 0.5$. When the nutrients inside the cell reach saturation, i.e., $d[n]/dt = 0$, we have $\kappa = \kappa_{specific}$.

Antibiotic Dynamics

The action of ribosome-targeting antibiotics is illustrated using the diagram in Figure 3A, which consists of two key components: the flux of antibiotics J_a entering the cell, and the binding of antibiotics to the active pool of ribosomes, r_a. The dynamics are described by the following set of equations, extending the model of Elf et al. (2006) and Greulich et al. (2015):

$$\begin{cases} da_{in}/dt = -\kappa a_{in} + f(r_a, r_b, a_{in}) + J_a(a_{ex}, a_{in}, A, V), \\ dr_a/dt = -\kappa r_a + f(r_a, r_b, a_{in}) + s, \\ dr_b/dt = -\kappa r_b - f(r_a, r_b, a_{in}), \end{cases} \tag{14}$$

where a_{ex} is the extracellular antibiotic concentration, a_{in} is the intracellular concentration of the antibiotic, r_a is the concentration of the active pool of ribosomes in the cell, r_b is concentration of the pool of ribosomes bound by the antibiotics, and s is the rate of synthesis of ribosomes. Unlike previous models (Elf et al., 2006; Greulich et al., 2015), here we account for the dependence of J_a on cell shape as

$$J_a(a_{ex}, a_{in}, A, V) = (P_{in}a_{ex} - P_{out}a_{in})\frac{A}{V}, \tag{15}$$

where P_{in} and P_{out} are the cell envelope permeabilities in the inward and outward directions, respectively. The ribosome-antibiotic interactions are defined by $f(r_a, r_b, a_{in}) = -k_{on}a_{in}(r_a - r_{min}) + k_{off}r_b$, where k_{on} is the rate of binding of antibiotics to ribosomes, and k_{off} is the rate of unbinding. These rate constants for chloramphenicol are known from Elf et al. (2006) and Greulich et al. (2015). Furthermore, cells produce more ribosomes to compensate for the inactive ribosomes bound by antibiotics (Scott et al., 2010). This is captured by the source term $s = \kappa[r_{max} - \kappa\Delta r(1/\kappa_{specific} - 1/\kappa_t\Delta r)]$, where $\Delta r = r_{max} - r_{min}$.

Cell-Shape Dynamics

Having described the dynamics of cell volume (Equation 1), division control (Equation 2), and nutrient and antibiotic transport (Equations 13 and 14), we need to additionally account for cell-surface-area synthesis to predict cell-shape changes. We assume that rate of synthesis cell surface area is proportional to cell volume (Harris and Theriot, 2016):

$$\frac{dA}{dt} = \beta V(t), \tag{16}$$

where β is the rate of surface area production, which depends on cell shape, growth rate, and the rate of division protein synthesis.

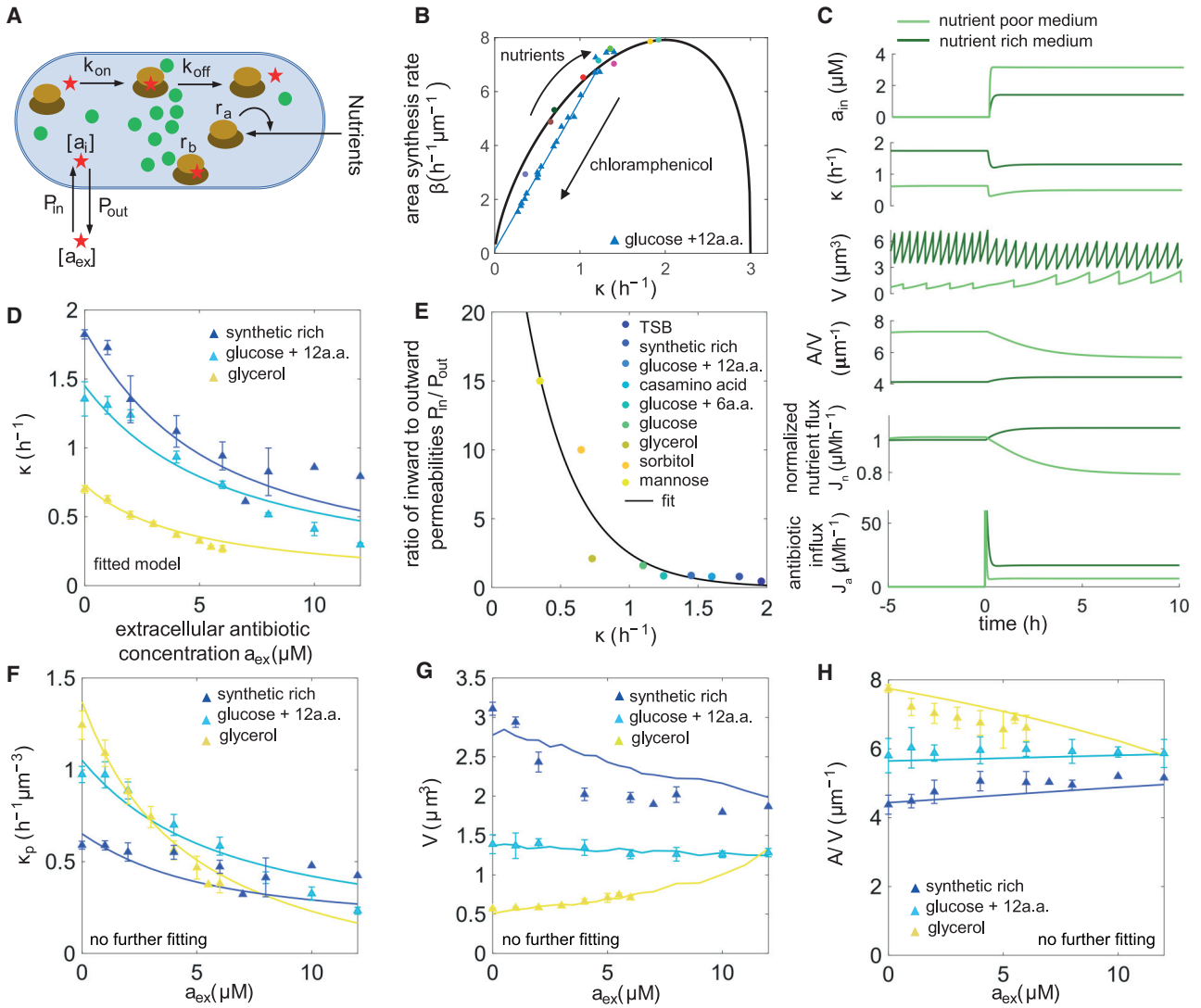

Figure 3. Cell-Shape Control under Translational Inhibition

(A) Schematic illustrating nutrient and antibiotic transport across the cell surface and antibiotic interactions inside the cell.

(B) Model predictions for the surface area synthesis rate (β) as a function of the growth rate (κ) for varying nutrient conditions, and its inhibition under chloramphenicol perturbations. β is calculated using $\beta = \kappa A/V$.

(C) Single-cell simulations of growth in response to a step pulse of chloramphenicol applied at $t = 0$ h in the extracellular medium. Top to bottom: dynamics of intracellular antibiotic concentration, growth rate, cell volume, surface-to-volume ratio, normalized nutrient, and antibiotic flux. Both nutrient and antibiotic fluxes are higher in rich media due to the increase in surface-to-volume ratio.

(D) Model growth inhibition curves fitted to experimental data (Si et al., 2017), to deduce the ratio of inward to outward cell-surface permeability. Data are represented as mean ± SEM.

(E) P_{in}/P_{out} increases with decreasing growth rate (quality of nutrients). We fit an exponential function (solid line) to the data for P_{in}/P_{out} at different nutrient conditions.

(F–H) Simulation results for the dependence of κ_p (F), average cell volume V (G), and average cell surface-to-volume ratio A/V (H) on chloramphenicol concentration, plotted against experimental data (Si et al., 2017) at three different nutrient conditions. Data are represented as mean ± SEM. See Tables 1 and 2 for a complete list of parameter values.

Solving Equations 1 and 16, one obtains $A/V = \beta/\kappa$, at steady state (Harris and Theriot, 2016). In recent work (Ojkic et al., 2019), we found that *E. coli* cells obey the relation: $A = \nu V^{2/3}$, under nutrient and translational perturbations, where ν is a geometric factor related to the cell aspect ratio η as $\nu = \eta\pi((\eta\pi/4) - (\pi/12))^{-2/3}$. Therefore, surface area production rate varies non-monotonically with growth rate as $\beta = \nu\kappa(\kappa/\kappa_p)^{-1/3}$ (Figure 3B).

Taken together, our model accounts for the key functions of ribosomes in controlling cell growth rate (κ), rate of production of

Table 2. List of Parameters Used in Antibiotic Simulations

Parameter	Value	Growth Medium	Expression/Method Used	Figure Number
$[n_{ext}]/\ n^*$	0.2	TSB	fitting $\kappa = \kappa_0[n]/([n]\ + n^*)$ when $\frac{d[n]}{dt} = 0$	Figures 3 and 4
	0.08	synthetic rich		
	0.03	glucose + 12 aa		
	0.05	casamino acid		
	0.018	glucose + 6 aa		
	0.008	glucose		
	0.002	glycerol		
$P_{out}(h^{-1}\ \mu m^{-1})$	20	all	$15 - 30\ h^{-1}$ (Greulich et al., 2015)	Figures 3 and 4
$P_{in}/\ P_{out}$	0.45	TSB	fitting growth inhibition curves	Figures 3 and 4
	0.80	synthetic rich		
	0.88	glucose + 12 aa		
	0.80	casamino acid		
	0.85	glucose + 6 aa		
	1.6	glucose		
	2.1	glycerol		
	10	sorbitol		
	15	mannose		
$k_{on}(\mu M^{-1}\ h^{-1})$	10	all	$1.08 - 13\ \mu M^{-1}\ h^{-1}$ (Greulich et al., 2015)	Figures 3 and 4
$k_D(\mu M)$	2.5	all	$0.5 - 5\ \mu M$ (Greulich et al., 2015)	Figures 3 and 4
$k_{off}(h^{-1}) = k_D k_{on}$	25	all	calculated	Figures 3 and 4

division proteins (κ_p), and the rate of surface area synthesis (β). Under translation inhibition, both κ and κ_p decreases as shown in Figures 2A and 2C. Surface area production rate is also impacted by translation inhibition, as shown in Figure 3B, albeit in a different manner from the growth rate. Differential reduction of κ and β under translation inhibition is indicative of changes in steady-state cell surface-to-volume ratio ($\propto \beta/\kappa$). To test this quantitatively, we simulated the coupled equations (STAR Methods) for single-cell growth (Equations 1, 2, and 16), nutrient (Equation 13), and ribosome-antibiotic dynamics (Equation 14) under stresses induced by ribosome-targeting antibiotics (Figure 3C). In response to a step pulse of antibiotic in a nutrient-rich medium at $t = 0$ h, the concentration of antibiotic inside the cell and the influx increases rapidly. This, in turn, reduced the cell elongation rate as a result of antibiotic binding to ribosomes, and leads to longer interdivision times, a decreased (increased) average birth volume, and a concomitant increase (decrease) in surface-to-volume ratio for cells growing in rich (poor) nutrient media. These results confirm our hypotheses that in nutrient poor media, cells reduce their surface-to-volume ratio to inhibit antibiotic influx, while in nutrient rich media, cells increase their surface-to-volume ratio to import more nutrients.

While all the model parameters can be calibrated from available experimental data (Tables 1 and 2; STAR Methods), the relative magnitude of the permeabilities, P_{in}/P_{out}, remains undetermined. To this end, we fit our model to the experimental growth-inhibition curves (Si et al., 2017) in different nutrient conditions (Figure 3D), treating P_{in}/P_{out} as a fitting parameter. Interestingly, we find that P_{in}/P_{out} is nutrient dependent and decreases with increasing specific growth rate (Figure 3E). As a result, J_n/J_a is an increasing function of growth rate, such that nutrient influx dominates over antibiotic influx in nutrient-rich media. Incorporating nutrient-dependent regulation of membrane permeability, our model predictions capture the experimental data for the decrease in division protein synthesis rate under chloramphenicol inhibition (Figure 3F) and the changes in cell volume (Figure 3G). Consistent with our hypothesis and experimental data, we find that cell surface-to-volume increases in nutrient-rich media ("synthetic rich" in experiments; Figure 3H). Conversely, in nutrient-poor medium (glycerol in experiments), cell surface-to-volume ratio reduces with increasing drug dosage, suggesting that cells are countering the influx of antibiotics if sufficient nutrients are not available.

Nutrient-dependent regulation membrane permeability to antibiotics (Figure 3E) can be a result of different metabolic pathways. It has been observed that *E. coli* cells have different metabolic pathways for nutrients depending on the growth conditions (de Groot et al., 2020). Furthermore, if the cells are subjected to a nutrient downshift, the proteome reallocates such that a larger fraction of proteins is allocated to the sector responsible for carbon catabolism, which in turn reduces the available proteome fraction for other sectors (Basan et al., 2015a; Mori et al., 2016). The transition from one metabolic mechanism to another can be justified using a proteome allocation model as suggested by Basan et al. (2015a) and Mori et al. (2016), or by increasing the glucose uptake rates. The drop in cell envelope permeability that we observe around $\kappa = 0.6\ h^{-1}$ (Figure 3E) matches the maximum growth rate that *E. coli* cells

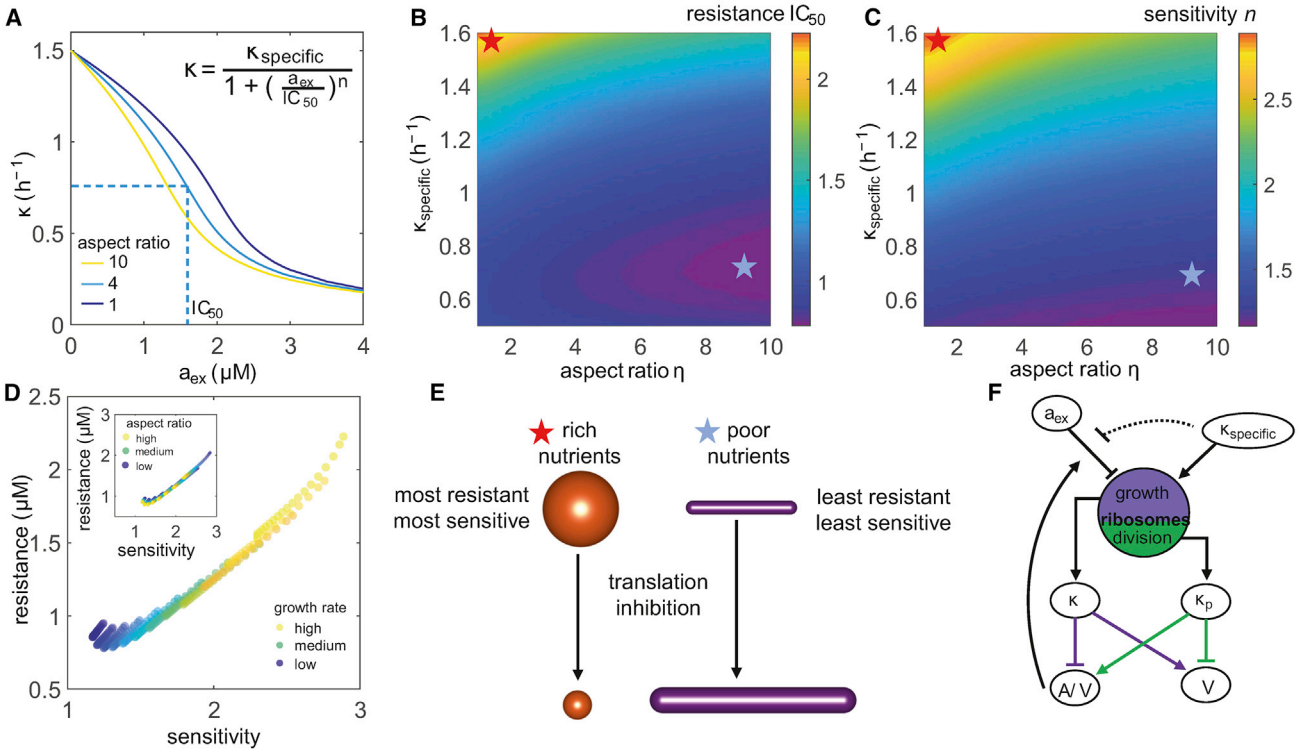

Figure 4. Cell Shape and Nutrient Quality Control Bacterial Resistance to Ribosome-Targeting Antibiotics

(A) Growth inhibition curves for three different values of cell aspect ratio in a nutrient-rich medium. Dashed line corresponds to IC_{50} on the x axis (i.e., the concentration of antibiotic when the growth rate reduces by half).

(B) Heatmap of IC_{50}, a metric for drug resistance, showing the effects of changing aspect ratio and nutrient quality. Red asterisk: maximally resistant; blue asterisk: least resistant.

(C) Heatmap of drug-dose sensitivity (n), showing the effects of changing cellular aspect ratio and nutrient quality of the growth medium.

(D) Correlation between drug resistance and dose sensitivity under changes in nutrient quality ($\kappa_{specific}$). Inset: correlation between drug resistance and dose sensitivity under changes in aspect ratio.

(E) Schematic illustrating fitness value for cell shapes and morphological changes that accompany bacterial response to translation inhibition in nutrient-rich and nutrient-poor growth media.

(F) Schematic representation of the feedback pathways that connect ribosomal translation to bacterial cell shape, growth, nutrient and antibiotic transport. See Tables 1 and 2 for a complete list of parameter values.

can achieve while staying below the critical limit on energy dissipation (Niebel et al., 2019).

Cell Surface Area Production Promotes Bacterial Growth Inhibition by Ribosome-Targeting Antibiotics

Our theory predicts that bacterial growth response to translation-inhibitory antibiotics is governed by nutrient-dependent cell-shape changes (Figures 2 and 3). To systematically study how bacterial growth inhibition depends on cell shape and nutrient quality, we simultaneously perturbed cell shape and ribosomal translation in varying growth media using our computational model. These simulations can be realized experimentally by simultaneously applying two antibiotics—one that changes cell shapes (e.g., by targeting the cell wall), and one that affects the translational machinery by inhibiting ribosomal activity. The resultant effect can be suppressive, antagonistic, or synergistic depending on what the combined effect of the two drugs is with respect to the individual effect of each (Bollenbach et al., 2009; Brochado et al., 2018).

In simulations, we simultaneously applied a surface area *modifier* and chloramphenicol to a cell growing at steady state. To achieve rounder cells, the modifier is a surface area synthesis inhibitor that decreases the surface production rate β, by decreasing the cell's geometric factor ν ($=A/V^{2/3}$), which in turn reduces cellular aspect ratio. By contrast, long filamentous cells are obtained when a surface area promoter is added (increasing ν), leading to cells with higher aspect ratios.

We investigated the response of growth rate to increasing chloramphenicol concentrations for cells with varying aspect ratios—ranging from $\eta = 1$ for coccoidal cells to $\eta = 10$ for filamentous cells (Figure 4A). The response of κ to the concentration of the applied antibiotic can be characterized by a Hill function of the form (Chevereau et al., 2015; Figure 4A)

$$\kappa(a_{ex}) = \frac{\kappa_{specific}}{1 + \left(\frac{a_{ex}}{IC_{50}}\right)^{n}}, \quad (17)$$

where IC_{50} is the half-inhibitory concentration of the antibiotic, and the Hill coefficient n quantifies the dose sensitivity of the growth rate to relative changes in drug concentration. We take IC_{50} as a measure of drug *resistance* (Chevereau et al., 2015).

For a range of aspect ratios and nutrient conditions, we fitted the growth inhibition curves to the Hill function in Equation 17, and obtained the values for IC_{50} (Figure 4B) and the dose sensitivity n (Figure 4C). Our model predicts that IC_{50} (resistance) increases with decreasing aspect ratio in nutrient-rich medium, while being less sensitive to changes in cell aspect ratio in nutrient-poor medium (Figure 4B). Dose sensitivity to changes in drug concentration increases with decreasing aspect ratio and increasing nutrient quality (Figure 4C), such that dose sensitivity is positively correlated with drug resistance (Figure 4D). These results indicate that cellular response to translation-inhibitory antibiotics is sensitive to both the nutrient quality as well as cell shape. We find that round coccoidal cells are the most drug resistant, while filamentous cells are the least resistant (Figure 4E). Furthermore, depending on nutrient quality, cellular morphological response to translation-inhibitory drugs is different. While cells increase their surface-to-volume ratio to import more nutrients in nutrient-poor medium, cells prefer to reduce their surface-to-volume ratio in nutrient-rich medium to inhibit antibiotic influx (Figures 2 and 3). These findings predict that bacterial growth inhibition can be maximized by simultaneously inhibiting ribosomal translation and promoting surface area production in nutrient-poor media.

DISCUSSION

We develop a whole-cell coarse-grained model for bacterial growth dynamics that connects intracellular control of translation with cell shape, division control, and extracellular environment. This provides a promising theoretical framework that quantitatively captures available experimental data for bacterial cell size and shape dynamics under nutrient and translational perturbations. Our study reveals that during nutrient shifts, the ribosomal resources are optimally allocated to maintain a balanced trade-off between the rates of cell growth and division protein (FtsZ) synthesis. In nutrient-rich media, more ribosomes are used for growth than division protein synthesis, leading to cell size inflation with increasing nutrient quality. Conversely in nutrient-poor media, cells allocate more ribosomal resources for division protein synthesis than growth, leading to a reduction in average cell size. This principle underlies the molecular basis for the celebrated *nutrient growth law* (Schaechter et al., 1958; Si et al., 2017), and can be interpreted as an optimization principle for cellular economy. Based on this principle, the resources allocated to a particular proteomic sector are inversely proportional to the efficiency of that sector (Pandey and Jain, 2016). In nutrient-rich media, cells invest more ribosomal resources to growth to compensate for a lower translational capacity. The latter can arise from an increased dilution rate of ribosomes under fast growth conditions, lowering the efficiency of protein synthesis. In nutrient-poor media, cells have a lower nutritional capacity that they compensate by allocating more resources to metabolism and division protein synthesis.

To explain the mechanistic origin of the ribosomal trade-off between growth and division protein synthesis, we propose a proteome allocation theory, extending the sector model introduced by Scott et al. (2010). In particular, we introduce a division protein sector X in the proteome, and derive a constitutive relation that the mass fraction of X, ϕ_X, is a linearly decreasing function of the mass fraction of ribosomes, ϕ_R. Existing experimental data support our model, and also falsify other possible models with X in the R-sector or the Q-sector. In particular, if X is the R- or Q-sector, we would expect cell size to always decrease under translation inhibition, a result that is inconsistent with experimental data (Basan et al., 2015b; Si et al., 2017). A recent study by Bertaux et al. (2020) also incorporated a division protein sector in a proteome model. In contrast to our theory, the authors assumed a phenomenological form for the dependence of ϕ_X on ϕ_P and ϕ_R: $\phi_X \propto \phi_P^{\alpha}\phi_R^{\beta}$, where the exponents α and β are deduced by fitting experimental data. The findings of Bertaux et al. (2020) are consistent with our results for cell size control under nutrient perturbations.

Our model for division control is chromosome agnostic and is thus inadequate for capturing the single-cell correlation patterns related to DNA replication initiation and segregation periods (Micali et al., 2018a; Grilli et al., 2018). However, we find that the rate of production of division proteins, κ_p, is proportional $(C+D)^{-1}$ (Figures S2A and S2B), where C is the duration from initiation to termination of one round of DNA replication, and D is the time period from replication termination to cell division. This relationship between adder protein synthesis and chromosome dynamics emerges from combining the principle of balanced biosynthesis $\kappa_p \propto \kappa$ (Si et al., 2019) with the relation $C+D \propto \kappa^{-1}$ (Helmstetter, 1996). The proportionality $\kappa_p \propto (C+D)^{-1}$ also emerges from the recent model suggested by Zheng et al. (2020) that cell size is linearly proportional to $\kappa(C+D)$. Using $V \propto \kappa(C+D)$ in conjunction with our theory $V \propto \kappa/\kappa_p$ also reveals $\kappa_p \propto (C+D)^{-1}$, consistent with experimental data (Si et al., 2019). However, we note that a linear relationship between cell size and $\kappa(C+D)$ does not accurately describe all available experimental data (Basan et al., 2015b; Si et al., 2017; Zhu et al., 2017) for cell size versus growth rate (Figure S2C).

Comparing our theory to experimental data, we uncover several feedback pathways among cell shape, growth rate, protein synthesis, and extracellular transport that were previously unknown (Figure 4F). In particular, we predict that under translation inhibition, cells break the balanced trade-off between ribosomes and division protein synthesis, leading to cell size inflation, reduction, or size invariance, in a nutrient-dependent manner. The model proposed by Bertaux et al. (2020) predicts that cell size always increases under translation inhibition, unless the cells followed a sizer-like law for cell size homeostasis. Our model predictions are in quantitative agreement with experimental data on *E. coli* cells subjected to chloramphenicol perturbations across various nutrient conditions (Si et al., 2017). If cells are grown in nutrient-rich media, the excess ribosomes produced under translation inhibition are allocated toward division, leading to smaller cell sizes and higher surface-to-volume ratios. This is in agreement with chloramphenicol-treated *E. coli* cells grown in synthetic rich medium. Conversely, in nutrient-poor

media cells allocate excess ribosomes toward growth, leading to cell size inflation and lower surface-to-volume ratios, in agreement with *E. coli* cell data in glycerol medium.

Our results suggest that changes in cell shape, in response to translation-inhibitory antibiotics, may confer certain fitness advantages under stress. In nutrient-rich media, it is more favorable for cells to reduce their surface-to-volume to minimize antibiotic influx. Whereas in nutrient-poor media, cells adapt to import more nutrients by increasing their surface-to-volume ratios. To quantitatively test the role of cell shape and nutrient quality on bacterial growth inhibition under antibiotic stress, we simulated bacterial growth under simultaneous perturbation of surface area production and translation inhibition in varying nutrient media. From growth-inhibition curves we measured bacterial response to antibiotics by quantifying resistance (half-inhibitory concentration of the drug) and dose sensitivity to increasing concentration of the drug. Our study reveals that that round-shaped cells are fitter and more drug resistant than higher-aspect-ratio filamentous cells, and that dose sensitivity increases with increasing nutrient quality. These results can be tested experimentally by measuring bacterial growth rates in response to simultaneous application of cell-wall targeting and ribosome-targeting antibiotics, in different nutrient concentrations. Interestingly, we predict that bacterial growth-inhibition can be maximized by simultaneously inhibiting ribosomal translation and promoting surface area production in nutrient-poor media.

STAR★METHODS

Detailed methods are provided in the online version of this paper and include the following:

- KEY RESOURCES TABLE
- RESOURCE AVAILABILITY
  - Lead Contact
  - Materials Availability
  - Data and Code Availability
- EXPERIMENTAL MODEL AND SUBJECT DETAILS
- METHOD DETAILS
  - Cell growth simulations
  - Proteome sector model
- QUANTIFICATION AND STATISTICAL ANALYSIS
  - Parameter determination

SUPPLEMENTAL INFORMATION

Supplemental Information can be found online at https://doi.org/10.1016/j.celrep.2020.108183.

ACKNOWLEDGMENTS

We thank Suckjoon Jun's lab (University of California, San Diego) for providing single-cell-shape data for *E. coli* and Guillaume Charras for many useful discussions. The authors thank the anonymous reviewers for many constructive comments and suggestions. S.B. acknowledges funding from EPSRC grant EP/R029822/1, Royal Society grants URF\R1\180187 and RGF\EA\181044, and National Science Foundation grant NSF PHY-2020295.

AUTHOR CONTRIBUTIONS

S.B. and D.S. conceived and designed research; D.S., N.O., and S.B. developed theory; D.S. performed simulations and analyzed data; and D.S. and S.B. wrote the paper.

DECLARATION OF INTERESTS

The authors declare no competing interests.

Received: February 24, 2020
Revised: June 24, 2020
Accepted: September 1, 2020
Published: September 22, 2020

REFERENCES

Adams, D.W., and Errington, J. (2009). Bacterial cell division: assembly, maintenance and disassembly of the Z ring. Nat. Rev. Microbiol. *7*, 642–653.

Amir, A. (2014). Cell size regulation in bacteria. Phys. Rev. Lett. *112*, 208102.

Banerjee, S., Lo, K., Daddysman, M.K., Selewa, A., Kuntz, T., Dinner, A.R., and Scherer, N.F. (2017). Biphasic growth dynamics control cell division in Caulobacter crescentus. Nat. Microbiol. *2*, 17116.

Basan, M., Hui, S., Okano, H., Zhang, Z., Shen, Y., Williamson, J.R., and Hwa, T. (2015a). Overflow metabolism in Escherichia coli results from efficient proteome allocation. Nature *528*, 99–104.

Basan, M., Zhu, M., Dai, X., Warren, M., Sévin, D., Wang, Y.-P., and Hwa, T. (2015b). Inflating bacterial cells by increased protein synthesis. Mol. Syst. Biol. *11*, 836.

Bertaux, F., Von Kügelgen, J., Marguerat, S., and Shahrezaei, V. (2020). A bacterial size law revealed by a coarse-grained model of cell physiology. bioRxiv. https://doi.org/10.1101/078998.

Bi, E.F., and Lutkenhaus, J. (1991). FtsZ ring structure associated with division in Escherichia coli. Nature *354*, 161–164.

Bollenbach, T., Quan, S., Chait, R., and Kishony, R. (2009). Nonoptimal microbial response to antibiotics underlies suppressive drug interactions. Cell *139*, 707–718.

Bremer, H., and Dennis, P.P. (1996). Modulation of chemical composition and other parameters of the cell by growth rate. E. Coli Salmonella Cell. Mol. Biol. *2*, 1553–1569.

Brochado, A.R., Telzerow, A., Bobonis, J., Banzhaf, M., Mateus, A., Selkrig, J., Huth, E., Bassler, S., Zamarreño Beas, J., Zietek, M., et al. (2018). Species-specific activity of antibacterial drug combinations. Nature *559*, 259–263.

Campos, M., Surovtsev, I.V., Kato, S., Paintdakhi, A., Beltran, B., Ebmeier, S.E., and Jacobs-Wagner, C. (2014). A constant size extension drives bacterial cell size homeostasis. Cell *159*, 1433–1446.

Chevereau, G., Dravecká, M., Batur, T., Guvenek, A., Ayhan, D.H., Toprak, E., and Bollenbach, T. (2015). Quantifying the determinants of evolutionary dynamics leading to drug resistance. PLoS Biol. *13*, e1002299.

de Groot, D.H., Lischke, J., Muolo, R., Planqué, R., Bruggeman, F.J., and Teusink, B. (2020). The common message of constraint-based optimization approaches: overflow metabolism is caused by two growth-limiting constraints. Cell. Mol. Life Sci. *77*, 441–453.

Deforet, M., van Ditmarsch, D., and Xavier, J.B. (2015). Cell-size homeostasis and the incremental rule in a bacterial pathogen. Biophys. J. *109*, 521–528.

Donachie, W.D. (1968). Relationship between cell size and time of initiation of DNA replication. Nature *219*, 1077–1079.

Ecker, R., and Schaechter, M. (1963). Bacterial growth under conditions of limited nutrition. Ann. N. Y. Acad. Sci. *102*, 549–563.

Elf, J., Nilsson, K., Tenson, T., and Ehrenberg, M. (2006). Bistable bacterial growth rate in response to antibiotics with low membrane permeability. Phys. Rev. Lett. *97*, 258104.

Flåtten, I., Fossum-Raunehaug, S., Taipale, R., Martinsen, S., and Skarstad, K. (2015). The DnaA protein is not the limiting factor for initiation of replication in Escherichia coli. PLoS Genet. *11*, e1005276.

Ghusinga, K.R., Vargas-Garcia, C.A., and Singh, A. (2016). A mechanistic stochastic framework for regulating bacterial cell division. Sci. Rep. *6*, 30229.

Greulich, P., Scott, M., Evans, M.R., and Allen, R.J. (2015). Growth-dependent bacterial susceptibility to ribosome-targeting antibiotics. Mol. Syst. Biol. *11*, 796.

Grilli, J., Cadart, C., Micali, G., Osella, M., and Cosentino Lagomarsino, M. (2018). The empirical fluctuation pattern of E. coli division control. Front. Microbiol. *9*, 1541.

Harris, L.K., and Theriot, J.A. (2016). Relative rates of surface and volume synthesis set bacterial cell size. Cell *165*, 1479–1492.

Harvey, R.J. (1973). Fraction of ribosomes synthesizing protein as a function of specific growth rate. J. Bacteriol. *114*, 287–293.

Helmstetter, C.E. (1996). Timing of synthetic activities in the cell cycle. E. Coli Salmonella Cell. Mol. Biol. *2*, 1627–1639.

Ho, P.-Y., and Amir, A. (2015). Simultaneous regulation of cell size and chromosome replication in bacteria. Front. Microbiol. *6*, 662.

Jun, S., and Taheri-Araghi, S. (2015). Cell-size maintenance: universal strategy revealed. Trends Microbiol. *23*, 4–6.

Jun, S., Si, F., Pugatch, R., and Scott, M. (2018). Fundamental principles in bacterial physiology-history, recent progress, and the future with focus on cell size control: a review. Rep. Prog. Phys. *81*, 056601.

Kaczanowska, M., and Rydén-Aulin, M. (2007). Ribosome biogenesis and the translation process in Escherichia coli. Microbiol. Mol. Biol. Rev. *71*, 477–494.

Kjeldgaard, N.O., Maaloe, O., and Schaechter, M. (1958). The transition between different physiological states during balanced growth of Salmonella typhimurium. J. Gen. Microbiol. *19*, 607–616.

Klumpp, S., Scott, M., Pedersen, S., and Hwa, T. (2013). Molecular crowding limits translation and cell growth. Proc. Natl. Acad. Sci. USA *110*, 16754–16759.

Maaløe, O. (1979). Regulation of the protein-synthesizing machinery-ribosomes, tRNA, factors, and so on. In Biological Regulation and Development: Gene Expression, R.F. Goldberger, ed. (Boston, MA: Springer US), pp. 487–542.

Männik, J., Walker, B.E., and Männik, J. (2018). Cell cycle-dependent regulation of FtsZ in Escherichia coli in slow growth conditions. Mol. Microbiol. *110*, 1030–1044.

Micali, G., Grilli, J., Marchi, J., Osella, M., and Cosentino Lagomarsino, M. (2018a). Dissecting the control mechanisms for DNA replication and cell division in E. coli. Cell Rep. *25*, 761–771.e4.

Micali, G., Grilli, J., Osella, M., and Lagomarsino, M.C. (2018b). Concurrent processes set E. coli cell division. Sci. Adv. *4*, eaau3324.

Miller, C., Thomsen, L.E., Gaggero, C., Mosseri, R., Ingmer, H., and Cohen, S.N. (2004). SOS response induction by β-lactams and bacterial defense against antibiotic lethality. Science *305*, 1629–1631.

Monod, J. (1949). The growth of bacterial cultures. Annu. Rev. Microbiol. *3*, 371–394.

Mori, M., Hwa, T., Martin, O.C., De Martino, A., and Marinari, E. (2016). Constrained allocation flux balance analysis. PLoS Comput. Biol. *12*, e1004913.

Niebel, B., Leupold, S., and Heinemann, M. (2019). An upper limit on Gibbs energy dissipation governs cellular metabolism. Nat. Metab. *1*, 125–132.

Ojkic, N., Serbanescu, D., and Banerjee, S. (2019). Surface-to-volume scaling and aspect ratio preservation in rod-shaped bacteria. eLife *8*, e47033.

Osella, M., Nugent, E., and Cosentino Lagomarsino, M. (2014). Concerted control of Escherichia coli cell division. Proc. Natl. Acad. Sci. USA *111*, 3431–3435.

Pandey, P.P., and Jain, S. (2016). Analytic derivation of bacterial growth laws from a simple model of intracellular chemical dynamics. Theory Biosci. *135*, 121–130.

Robert, L. (2015). Size sensors in bacteria, cell cycle control, and size control. Front. Microbiol. *6*, 515.

Ruusala, T., Andersson, D., Ehrenberg, M., and Kurland, C.G. (1984). Hyperaccurate ribosomes inhibit growth. EMBO J. *3*, 2575–2580.

Sauls, J.T., Li, D., and Jun, S. (2016). Adder and a coarse-grained approach to cell size homeostasis in bacteria. Curr. Opin. Cell Biol. *38*, 38–44.

Sauls, J.T., Cox, S.E., Do, Q., Castillo, V., Ghulam-Jelani, Z., and Jun, S. (2019). Control of Bacillus subtilis replication initiation during physiological transitions and perturbations. MBio *10*, e02205–e02219.

Schaechter, M. (2006). From growth physiology to systems biology. Int. Microbiol. *9*, 157–161.

Schaechter, M., Maaloe, O., and Kjeldgaard, N.O. (1958). Dependency on medium and temperature of cell size and chemical composition during balanced grown of Salmonella typhimurium. J. Gen. Microbiol. *19*, 592–606.

Scott, M., Gunderson, C.W., Mateescu, E.M., Zhang, Z., and Hwa, T. (2010). Interdependence of cell growth and gene expression: origins and consequences. Science *330*, 1099–1102.

Scott, M., Klumpp, S., Mateescu, E.M., and Hwa, T. (2014). Emergence of robust growth laws from optimal regulation of ribosome synthesis. Mol. Syst. Biol. *10*, 747.

Sekar, K., Rusconi, R., Sauls, J.T., Fuhrer, T., Noor, E., Nguyen, J., Fernandez, V.I., Buffing, M.F., Berney, M., Jun, S., et al. (2018). Synthesis and degradation of FtsZ quantitatively predict the first cell division in starved bacteria. Mol. Syst. Biol. *14*, e8623.

Si, F., Li, D., Cox, S.E., Sauls, J.T., Azizi, O., Sou, C., Schwartz, A.B., Erickstad, M.J., Jun, Y., Li, X., and Jun, S. (2017). Invariance of initiation mass and predictability of cell size in Escherichia coli. Curr. Biol. *27*, 1278–1287.

Si, F., Le Treut, G., Sauls, J.T., Vadia, S., Levin, P.A., and Jun, S. (2019). Mechanistic origin of cell-size control and homeostasis in bacteria. Curr. Biol. *29*, 1760–1770.e7.

Söderström, B., Badrutdinov, A., Chan, H., and Skoglund, U. (2018). Cell shape-independent FtsZ dynamics in synthetically remodeled bacterial cells. Nat. Commun. *9*, 4323.

Stouthamer, A.H., and Bettenhaussen, C. (1973). Utilization of energy for growth and maintenance in continuous and batch cultures of microorganisms. A reevaluation of the method for the determination of ATP production by measuring molar growth yields. Biochim. Biophys. Acta *301*, 53–70.

Taheri-Araghi, S., Bradde, S., Sauls, J.T., Hill, N.S., Levin, P.A., Paulsson, J., Vergassola, M., and Jun, S. (2015). Cell-size control and homeostasis in bacteria. Curr. Biol. *25*, 385–391.

Vadia, S., and Levin, P.A. (2015). Growth rate and cell size: a re-examination of the growth law. Curr. Opin. Microbiol. *24*, 96–103.

Wallden, M., Fange, D., Lundius, E.G., Baltekin, Ö., and Elf, J. (2016). The synchronization of replication and division cycles in individual E. coli cells. Cell *166*, 729–739.

Yin, J. (2004). Genome function—a virus-world view. In Advances in Systems Biology, L.K. Opresko, J.M. Gephart, and M.B. Mann, eds. (Boston, MA: Springer US), pp. 31–46.

Young, K.D. (2006). The selective value of bacterial shape. Microbiol. Mol. Biol. Rev. *70*, 660–703.

Zaslaver, A., Kaplan, S., Bren, A., Jinich, A., Mayo, A., Dekel, E., Alon, U., and Itzkovitz, S. (2009). Invariant distribution of promoter activities in Escherichia coli. PLoS Comput. Biol. *5*, e1000545.

Zheng, H., Bai, Y., Jiang, M., Tokuyasu, T.A., Huang, X., Zhong, F., Wu, Y., Fu, X., Kleckner, N., Hwa, T., and Liu, C. (2020). General quantitative relations linking cell growth and the cell cycle in Escherichia coli. Nat. Microbiol. *5*, 995–1001.

Zhu, M., Dai, X., Guo, W., Ge, Z., Yang, M., Wang, H., and Wang, Y.-P. (2017). Manipulating the bacterial cell cycle and cell size by titrating the expression of ribonucleotide reductase. mBio *8*, e01741–17.

STAR★METHODS

KEY RESOURCES TABLE

REAGENT or RESOURCE	SOURCE	IDENTIFIER
Deposited Data		
E. coli data	Si et al., 2017	https://doi.org/10.1016/j.cub.2017.03.022
E. coli data	Taheri-Araghi et al., 2015	https://doi.org/10.1016/j.cub.2014.12.009
E. coli data	Si et al., 2019	https://doi.org/10.1016/j.cub.2019.04.062
E. coli data	Zhu et al., 2017	https://doi.org/10.1128/mBio.01741-17
E. coli data	Zheng et al., 2020	https://doi.org/10.1038/s41564-020-0717-x
E. coli data	Basan et al., 2015a, 2015b	https://doi.org/10.15252/msb.20156178
Software and Algorithms		
MATLAB	MathWorks	https://uk.mathworks.com/

RESOURCE AVAILABILITY

Lead Contact

Further information and requests for data should be directed to and will be fulfilled by the Lead Contact, Shiladitya Banerjee (shiladtb@andrew.cmu.edu).

Materials Availability

This study did not generate new unique reagents or materials.

Data and Code Availability

Analyzed datasets generated in this study can be found at https://github.com/BanerjeeLab/CellReports2020. Code supporting the current study are available from the corresponding author upon reasonable request.

EXPERIMENTAL MODEL AND SUBJECT DETAILS

Single-cell size, shape and growth data for *Escherichia coli* are obtained from Taheri-Araghi et al. (2015) and population-averaged data are analyzed from Si et al. (2017). In Figures 1, 2, and 3 we analyze data for *E. coli* strain NCM3722. Figure S2C uses cell volume data for NCM3722 strain (Si et al., 2017; Basan et al., 2015b; Zhu et al., 2017), MG1655 strain (Si et al., 2017), AMB1655 strain (Zheng et al., 2020) and RNR titration strain FL-2 (Zhu et al., 2017).

METHOD DETAILS

Cell growth simulations

To investigate the dynamic response of cell shape and growth to applied antibiotic and nutrient shifts, we simulated single-cell growth over multiple generations. We first initiated cells at random stages in their cell cycle, and upon division followed the daughter cells over a number of generations until steady-state is reached. During each cell generation i, we evolved the following seven coupled differential equations for cell volume V_i, division protein abundance X_i, surface area A_i, nutrient concentration inside the cell $[n_i]$, antibiotic concentration inside the cell a^i_{in}, active ribosomes r^i_a, and inactive or antibiotic-bound ribosomes, r^i_b.

$$\frac{dV_i}{dt} = \kappa(r^i_a)V_i(t), \tag{18}$$

$$\frac{dX_i}{dt} = \kappa_p(r^i_a)V_i(t) - \mu X_i(t), \tag{19}$$

$$\frac{dA_i}{dt} = \beta(r^i_a)V_i(t), \tag{20}$$

$$\frac{d[n_i]}{dt} = J_n([n_i], A_i, V_i) - \kappa(r_a^i)[n_i] - \kappa_r r_a^i, \tag{21}$$

$$\frac{da_{\text{in}}^i}{dt} = -\kappa(r_a^i)a_{\text{in}}^i + f(a_{\text{in}}^i, r_a^i, r_b^i) + J_a(a_{\text{in}}^i, [n_i], A_i, V_i), \tag{22}$$

$$\frac{dr_a^i}{dt} = -\kappa(r_a^i)r_a^i + f(a_{\text{in}}^i, r_a^i, r_b^i) + s(r_a^i, [n_i]), \tag{23}$$

$$\frac{dr_b^i}{dt} = -\kappa(r_a^i)r_b^i - f(a_{\text{in}}^i, r_a^i, r_b^i). \tag{24}$$

In the above equations, we have (dropping 'i' for simplicity):

$$\kappa(r_a) = \kappa_t(r_a - r_{\min}).$$

$$\kappa_p(r_a) = \kappa_p^0(r_{\max}^* - r_a).$$

$$\beta(r_a) = \nu[\kappa(r_a)]^{2/3}[\kappa_p(r_a)]^{1/3}.$$

$J_n(A, V, [n]) = [n_{\text{ext}}]P_{\text{in}}([n])A/V$, where $[n_{\text{ext}}]$ is the extracellular nutrient concentration, and $P_{\text{in}}([n])$ is the nutrient-dependent inward permeability (Figure 3E)

$$f(a_{\text{in}}, r_a, r_b) = -k_{\text{on}}a_{\text{in}}(r_a - r_{\min}) + k_{\text{off}}r_b.$$

$$J_a(a_{\text{in}}, [n], A, V) = (P_{\text{in}}([n])a_{\text{ex}} - P_{\text{out}}a_{\text{in}})A/V.$$

$$s(r_a, [n]) = \kappa(r_a)\left(r_{\max} - \kappa(r_a)(r_{\max} - r_{\min})\left(\kappa_{\text{specific}}([n])^{-1} - 1\Big/\kappa_t(r_{\max} - r_{\min})\right)\right).$$

$$\kappa_{\text{specific}}([n]) = \kappa_0[n]/([n] + n^*).$$

For each cell cycle i, Equations 18 to 24 are evolved for $t \leq \tau_i$, where τ_i is the interdivision time for the i^{th} generation. Division is triggered when $X_i = X_0$, with X_0 a constant. Upon division, we set: $V_{i+1}(0) = D_R V_i(\tau_i)$, $X_{i+1}(0) = 0$, $A_{i+1}(0) = D_R A_i(\tau_i)$, $[n_{i+1}](0) = [n_i](\tau_i)$, $a_{\text{in}}^{i+i}(0) = a_{\text{in}}^i(\tau_i)$, $r_a^{i+1}(0) = r_a^i(\tau_i)$, $r_b^{i+1}(0) = r_b^i(\tau_i)$, where D_R is a Gaussian random variable with mean 0.5 and standard deviation 0.05. We initialize the nutrient concentration inside the cell ($[n_i]$) close to zero, and calibrate the extracellular nutrient concentration $[n_{\text{ext}}]$ to reach the growth rate of the medium we choose to simulate. Over time $[n_i]$ reaches the steady-state value $n^*\kappa_{\text{specific}}/(\kappa_0 - \kappa_{\text{specific}})$, such that $\kappa = \kappa_{\text{specific}}$. We run simulations for additional 5h after the nutrient concentration reaches steady-state, to record the average values of cell volume, area, and ribosome concentration. Antibiotic perturbation is applied after 10h from the start of the simulations and continued for another 20h, when we compute the average values for the various cellular variables.

Proteome sector model

The total mass of division proteins, M_X, increases at a rate proportional to the amount of actively translating ribosomes, N_R^{active},

$$\frac{dM_X}{dt} = af_X k_t N_R^{\text{active}}, \tag{25}$$

where $N_R^{\text{active}} = N_R - N_R^{\min}$, N_R is the total number of ribosomes, $N_R^{\min}$ is the number of ribosomes not participating in protein synthesis, k_t is the rate of translation per ribosome, f_X is the fraction of ribosomes devoted to synthesizing X, and a is the concentration of amino acids. Similarly, $dM_R/dt = af_R k_t N_R^{\text{active}}$, $dM_P/dt = af_P k_t N_R^{\text{active}}$, and $dM_Q/dt = af_Q k_t N_R^{\text{active}}$, where M_R, M_P and M_Q are masses of R, P and

Q sector proteins, f_P, f_R, and $f_Q = 1 - f_R - f_X - f_P$ are the mass fractions of ribosomes devoted to synthesizing each of these sectors. Therefore, the total dry mass of the cell, $M = M_P + M_X + M_R + M_Q$, increases at a rate proportional to the number of active ribosomes,

$$\frac{dM}{dt} = ak_t N_R^{\text{active}} . \tag{26}$$

If m_R is the mass of individual ribosomes, we get,

$$\frac{dM_X}{dt} = af_X k_t \left(M_R - M_R^{\min}\right) \Big/ m_R . \tag{27}$$

The instantaneous mass fraction of X, $\phi_X(t) = M_X(t)/M(t)$, then satisfies:

$$\frac{d\phi_X}{dt} + \kappa\phi_X = \frac{f_X k_t}{m_R} a\left(\phi_R - \phi_R^{\min}\right) , \tag{28}$$

where ϕ_R is the mass of fraction of ribosomes. At steady-state $\phi_X = f_X$, using the relation: $\kappa = k_t a(\phi_R - \phi_R^{\min})/m_R$. We can rewrite the above equation in terms of the concentration of X, $c_X = \phi_X \rho_c / m_x$, where ρ_c is the mass density of the cell, and m_x is the mass of an individual X molecule. This gives us,

$$\frac{dc_X}{dt} + \kappa c_X = \frac{f_X k_t m_x}{m_R \rho_c} a\left(\phi_R - \phi_R^{\min}\right) . \tag{29}$$

Using $X = c_X V$, where X is total amount of division proteins in the cell, we derive dynamics of division protein accumulation,

$$\frac{dX}{dt} = \frac{f_X k_t m_x}{m_R \rho_c} a\left(\phi_R - \phi_R^{\min}\right) V . \tag{30}$$

The above equation allows us to identify the division protein production rate as,

$$k_p = \frac{f_X k_t m_x}{m_R \rho_c} a\left(\phi_R - \phi_R^{\min}\right) . \tag{31}$$

The steady-state concentration of amino acids is determined by the balance between the rate of nutrient influx by transporters and the rate of translation by active ribosomes (Scott et al., 2014),

$$\frac{da}{dt} = k_n \phi_P - a\kappa_t \left(\phi_R - \phi_R^{\min}\right) , \tag{32}$$

where ϕ_P is the mass fraction of P-sector metabolic proteins, and $\kappa_t = k_t a \rho / m_R$. At steady-state, we have $a(\phi_R - \phi_R^{\min}) = k_n \phi_P / \kappa_t$. Using $\phi_X = \phi_R^{\max} - \phi_R - \phi_P$, we obtain

$$\phi_R = \frac{1}{\kappa_n + \kappa_t} \left(\phi_R^{\max} \kappa_n + \kappa_t \phi_R^{\min} - \phi_X \kappa_n\right) , \tag{33}$$

where $\kappa_n = k_n / a$. Therefore, $k_p \propto \phi_X \phi_P = \phi_X(\phi_R^{\max} - \phi_R - \phi_X) \approx \phi_X(\phi_R^{\max} - (\phi_R^{\max}\kappa_n + \kappa_t \phi_R^{\min})/(\kappa_n + \kappa_t))$, assuming that ϕ_X occupies a small fraction of the proteome. We thus get: $k_p \approx \phi_X (m_x / \rho_c \rho) \kappa_n \kappa_t (\phi_R^{\max} - \phi_R^{\min})/(\kappa_t + \kappa_n)$. In terms of ribosome mass fraction, the rate of production of division proteins is then given by:

$$k_p = \frac{m_x \kappa_t}{\rho_c \rho} \left(\phi_R^{\max} - \phi_R^{\min}\right) \left(\frac{\kappa_n \phi_R^{\max} + \kappa_t \phi_R^{\min}}{(\kappa_n + \kappa_t)} - \phi_R\right) . \tag{34}$$

QUANTIFICATION AND STATISTICAL ANALYSIS

Parameter determination

We extracted the parameters κ_t and $r_{\min}$ by fitting the equation $\kappa = \kappa_t (r - r_{\min})$ to the data for growth rate versus RNA/protein ratio (Si et al., 2017; Table 1). Using our theoretical model, we obtained the expression for cell volume V as a function of r (Equation 5), which we fitted to experimental data (Si et al., 2017), in order to to extract the parameters κ_p^0, $r_{\max}^*$ and μ (Table 1). For cells under Chloramphenicol stress, the nutrient-dependent parameters κ_n and δr were obtained by fitting Equations 10 and 11 to the experimental dataset for each nutrient condition (Table 1). From experimental data (Si et al., 2017), we estimated the division protein production rate as $\kappa_p = \kappa / \langle V \rangle$. To determine the permeability of the cell envelope to nutrient and antibiotic transport, we fitted the growth inhibition curves resulting from our simulations to the growth inhibition curves from the data in Si et al. (2017), using a method of least-squares. We find that $P_{\text{in}}/P_{\text{out}}$ is a function of nutrient quality, and used that as an input to our model simulations. Tables 1 and 2 list a complete set of parameter values used in our model simulations. Note that there are free parameters in the model, which include: X_0, n^* and κ_0. We do not use X_0 directly, as the parameter is absorbed in κ_p by renormalizing the number of division proteins by X_0 i.e., $X(t = 0) = 0$

and $X(t = \tau) = X_0 = 1$. We determine the nutrient specific growth rate by treating $[n_{ext}]/n^*$ as a fitting parameter. To this end, we arbitrarily pick the values for n^* and κ_0 and let the nutrients inside the cell to reach steady-state, $d[n]/dt = 0$. The steady-state value for $[n]$ depends on $[n_{ext}]$ and determines the nutrient-specific growth rate $\kappa = \kappa_{specific} = \kappa_0[n]/(n^* + [n])$. For each growth medium, we tune the value of $[n_{ext}]/n^*$ such that it results in the value of κ equal to the growth rate reported in experiments.